Composites Part B 99 (2016) 196–202

Contents lists available at ScienceDirect

Composites Part B

journal homepage: www.elsevier.com/locate/compositesb

Using ultrasound-assisted dispersion and in situ emulsion polymerization to synthesize TiO_2/ASA (acrylonitrile-styrene-acrylate) nanocomposites

Bo Xiang [a, b], Jun Zhang [a, b, *]

[a] Department of Polymer Science and Engineering, College of Materials Science and Engineering, Nanjing Tech University, Nanjing 210009, China
[b] Jiangsu Collaborative Innovation Center for Advanced Inorganic Function Composites, Nanjing 210009, China

ARTICLE INFO

Article history:
Received 24 February 2016
Received in revised form
20 May 2016
Accepted 3 June 2016
Available online 6 June 2016

Keywords:
Polymer-matrix composites (PMCs)
Fracture toughness
Mechanical properties
Electron microscopy

ABSTRACT

In this study, TiO_2/acrylonitrile-styrene-acrylate (ASA) nanocomposites with different loading content of TiO_2 were prepared via in situ emulsion polymerization. Before the polymerization, TiO_2 nanoparticles were dispersed in the reaction monomer by ultrasonic to reduce the agglomeration of TiO_2. A series of characterization were taken to study the properties of the nanocomposites. The result of Wide angle X-ray diffraction (WAXD) analysis indicated that the crystal form of TiO_2 remained unchanged after the in situ emulsion polymerization. Interestingly, the introduction of TiO_2 induced a significant improvement in the impact toughness of TiO_2/ASA nanocomposites, which increased dramatically by about 10 kJ/m^2 compared with neat ASA. And we attributed this improvement to the better dispersibility of TiO_2 in ASA matrix which is proved by Transmission Electron Microscopy (TEM) analysis. In addition, the solar reflectance of the nanocomposites was related to the addition of TiO_2 nanoparticles. The more the TiO_2 nanoparticle was added, the higher the solar reflectance of the nanocomposite was. Moreover, the outdoor temperature test just proved the result of the solar reflectance.

1. Introduction

In recent years, the organic/inorganic nanocomposites or hybrid materials have attracted extensive attention as they represent pretty excellent chemical and physical properties [1–4]. Clearly, The obtained nanocomposites or hybrid materials might offer the opportunity to combine the desirable properties of both organic polymer and inorganic solid [5,6]. Titanium dioxide (TiO_2) is often used as the inorganic filler particles in the composite preparation for its excellent weatherability, chemical stability, thermal stability and intensive ultraviolet absorption [7,8].

Acrylonitrile-styrene-acrylic (ASA) terpolymer prepared by grafting copolymerization of styrene and acrylonitrile monomers onto acrylic rubber particles was developed in the 1970s as an impact-resistance thermoplastic [9]. ASA has a similar structure with acrylonitrile-butadiene-styrene (ABS) terpolymer expect the butadiene rubber was replaced by acrylic rubber, which can resolve the physical (or chemical) aging of butadiene rubber [10]. Therefore, ASA has many excellent properties, such as good toughness, dimensional stability, aging and weatherability and thermal stability, for which ASA is used in a wide variety of applications including outdoor materials, automobile, electronics and so on. If we introduce the inorganic TiO_2 nanoparticles to ASA polymeric matrix to form TiO_2/ASA nanocomposite, it might lead to some much better properties. Melt blending is an easy and common way to prepare hybrid composites containing TiO_2 nanoparticles [11–14]. However, some disadvantages such as the agglomeration of TiO_2 in polymeric matrix will negatively affect some properties of the hybrid composites [14,15]. Xu et al. had prepared the composite of TiO_2 and ASA by solution mixing, and they improved the dispersibility and compatibility of TiO_2 in ASA matrix by surface organic modification of TiO_2. Finally, the UV absorption properties as well as the heat resistance and the acid and alkali resistance of the composite were all improved [16]. Here, we try another way, that is in situ emulsion polymerization, to prepare TiO_2/ASA nanocomposites.

In our present work, TiO_2/ASA nanocomposites with different loading content of TiO_2 were prepared by in situ emulsion

* Corresponding author. Department of Polymer Science and Engineering, College of Materials Science and Engineering, Nanjing Tech University, Nanjing 210009, China.
E-mail address: zhangjun@njtech.edu.cn (J. Zhang).

http://dx.doi.org/10.1016/j.compositesb.2016.06.012
1359-8368/

polymerization. Before the polymerization, TiO_2 nanoparticles were dispersed in the reaction monomer by ultrasonic to reduce the agglomeration of TiO_2. Among all the characterization, we focused on the influence of introduced TiO_2 nanoparticles on the mechanical and cooling properties of TiO_2/ASA nanocomposites.

2. Experimental

2.1. Materials

The titanium dioxide (TiO_2 R902) powder was a product from DuPont Company, America. N-butyl acrylate (BA, CP) and styrene (St, CP) were both purchased from Shanghai LingFeng chemical reagent Company Limited, China. Acrylonitrile (AN, CP) was received from Yixing Lilai Chemical Company Limited, China. Distillated deionized water (DDI) was commercially obtained from Nanjing Wanqing Chemical Classware Istrument Company Limited, China. Allyl methacrylate (AMA, AR) was supplied by Aladdin Chemistry Company Limited, China. Tert-Dodecylmercaptan (TDM, CP) was purchased from Sinopharm Chemical Reagent Company Limited, China. Sodium dodecyl sulfonate (SDS, CP), ammonium persulfate (APS, AR) and sodium hydroxide (NaOH, AR) were also purchased from Shanghai LingFeng chemical reagent Company Limited, China. BA, St, and AN were firstly distilled at a reduced pressure before use.

2.2. Synthesis of TiO_2/ASA nanocomposite emulsion

TiO_2/ASA nanocomposite emulsion was synthesized by adding TiO_2 nanoparticles during in situ emulsion polymerization. The schematic diagram for the preparation of TiO_2/ASA nanocomposite emulsion is shown in Scheme 1. And the whole synthetic process could be divided into the following three stages. The first stage is to synthesize PBA seed latexes. Different amounts (0, 1, 2 and 3 wt% of total monomer) of TiO_2 nanoparticles was dispersed into 30 g of BA monomer by ultrasonic disperser (NH-1000, Shanghai Hanuo Instrument Company Limited, China) for 30 min, while a certain amount of SDS and $NaHCO_3$ were dissolved in DDI. Then the dispersion and the aqueous were mixed by mechanical stirring in a four-neck flask equipped with a reflux condenser, a nitrogen inlet, a thermometer, and a mechanical stirrer. The mixture was stirred at room temperature for several hours. Next, the initiator APS was added drop wise to the reaction mixture, and the polymerization was carried out at about 70 °C in an oil bath for 3.5 h under nitrogen atmosphere. The second stage is to enlarge the particles of PBA and synthesize PBA core latexes. A certain amount of BA pre-emulsion, APS and $NaHCO_3$ were complementally added, and polymerized at the same reaction condition as above. The last stage is to synthesize TiO_2/ASA latexes. The pre-emulsion of St and AN, a certain amount of APS, $NaHCO_3$ and chain transfer agent TDM were complementally added, and polymerized at the same reaction condition as above. the specific recipes are listed in Table 1.

2.3. Sample preparation

The synthesized TiO_2/ASA nanocomposite latexes were dried in

Table 1
Recipes of the three stages for preparation of TiO_2/ASA latexes.

Ingredients	The first stage (g)	The second stage (g)	The last stage (g)
TiO_2	0/1.5/3.0/4.5	–	–
St	30	60	–
BA	–	–	45
AN	–	–	15
DDI	150	180	90
APS	0.075	0.09	0.15
SDS	0.0654	0.0784	0.0392
TDM	–	–	0.06
$NaHCO_3$	0.1	0.2	0.2

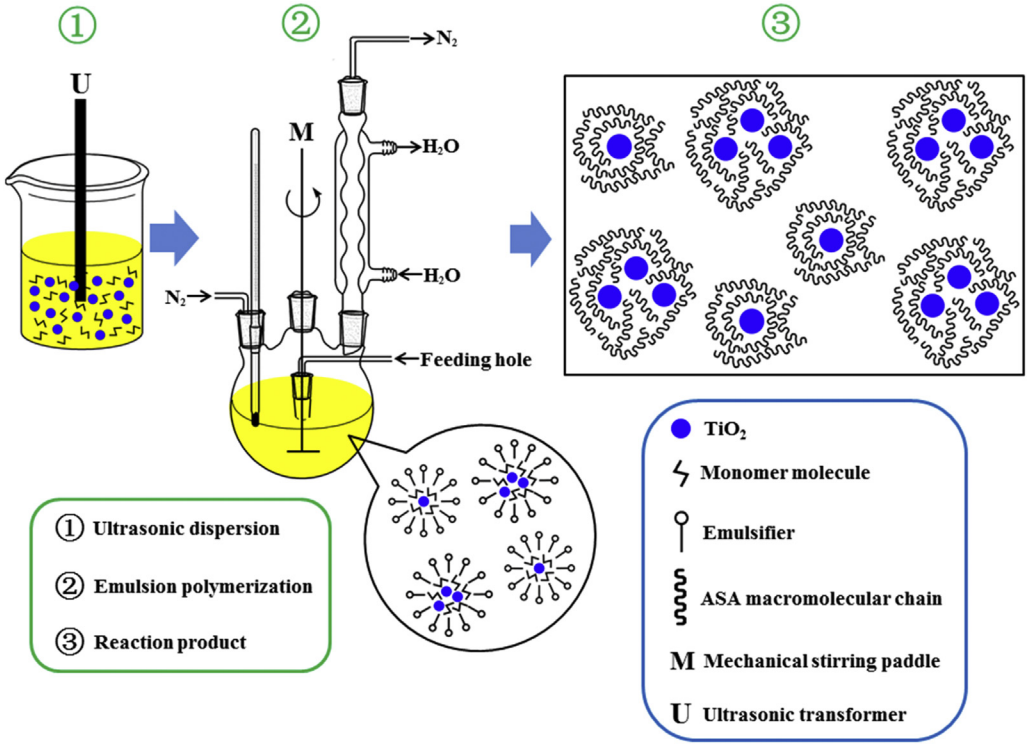

Scheme 1. Schematic diagram for the preparation of TiO_2/ASA nanocomposite emulsion.

tetrafluoroethylene molds for 5 h. Then, the dried TiO_2/ASA nanocomposites were fused in a two-roll mill at 180 °C to remove the micromolecules, followed by molding into sheets of approximately 30 μm, 1 mm and 4 mm in thickness by compression-molding at 175 °C. The sheets of approximately 30 μm thickness were prepared for Fourier transform infrared (FTIR) tests. The dumb-bell shaped pieces cut from 1-mm sheets were used for tensile test. Rectangular samples (80 × 10 × 4 mm^3) were machined for impact test.

2.4. Characterization

2.4.1. Transmission Electron Microscopy (TEM) analysis

TEM was used to observe the dispersibility of TiO_2 in ASA matrix. The morphology of the latexes were observed using a transmission electron microscope (JEM-1011, JEOL, Japan) with an accelerating voltage of 100 kV. The latexes were further diluted with DDI, and then diluted droplets were transferred onto the copper grids, mesh 200, and dried in open air.

2.4.2. FTIR spectra analysis

The transmittance infrared spectroscopy was obtained by a FTIR spectrometer (Nexus 670, Nicolet, USA). And the testing condition was set at the resolution of 4 cm^{-1} with 32 scans for each spectrum in the range of 4000–400 cm^{-1}.

2.4.3. Wide angle X-ray diffraction (WAXD) measurement

WAXD patterns were recorded on a Rigaku Smart Lab 3000 diffractometer (MiniFlex 600, Rigaku, Japan) using Cu K_α radiation (35 kV/30 mA). Scanning was performed from 5° to 80° at a rate of 10°/min.

2.4.4. Mechanical properties

The test of Notched Izod impact strength was carried out on an Izod impact tester (UJ-4, Chengde Machine Factory, China) at room temperature according to ISO 180. The tensile property was evaluated using a universal testing machine (CMT 5254, Shenzhen SANS testing machine, Co., Ltd., China) at stable rates of 5 mm/min following ISO 527.

2.4.5. Scanning electron microscopy (SEM) analysis

The morphology of the impact-fractured surfaces of ASA and TiO_2/ASA nanocomposites was observed through a SEM apparatus (JSM-7600F; JEOL, Japan) with a working voltage of 15 kV. The fracture surfaces of blends were coated with a thin conductive layer of gold before scanning.

2.4.6. Ultraviolet–Visible–near infrared (UV–Vis–NIR) spectral measurement

The UV–vis–NIR spectral measurement was conducted by a spectrometer with an integrating sphere (Shimadzu UV-3600, Japan). The spectral region used to conduct the solar reflectance and transmittance was from 280 to 2500 nm. Barium sulfate was used as a white reference. The reflectance of each region in solar irradiation can be calculated by the following equation [17,18]:

$$R_{\lambda_0\to\lambda_1} = \left[\int_{\lambda_1}^{\lambda_0} r(\lambda)i(\lambda)d\lambda\right] \Big/ \left[\int_{\lambda_1}^{\lambda_0} i(\lambda)d\lambda\right] \quad (1)$$

where $R_{\lambda_0\to\lambda_1}$ is the reflected fraction of solar irradiation incident at wavelengths between λ_0 and λ_1, and $R_{\lambda_0\to\lambda_1}$ is the irradiance-weighted average of its spectral reflectance $r(\lambda)$, $i(\lambda)$ is the solar spectral irradiance (power per unit area per unit wavelength).

The irradiance-weighted average reflectance included solar reflectance R_{sol} (280–2500 nm), UV reflectance R_u (280–400 nm), visible reflectance R_v (400–700 nm), and NIR reflectance R_n (700–2500 nm). The total solar reflectance can be calculated by the following equation, which is based on the aforementioned distribution of each solar power (5% UV, 43% visible, and 52% NIR) yield [17,18],

$$R_{sol} = 0.05R_u + 0.43R_v + 0.52R_n \quad (2)$$

2.4.7. Temperature test

To evaluate the real cooling property of the nanocomposites, we have designed a sandwich structure device [19]. The experiment was performed in a sunny day at noon (from 12:00–13:00). The inner temperature is read during a certain time interval.

3. Results and discussion

3.1. TEM analysis

TEM has proven to be a powerful tool for studying the dispersion of inorganic nanoparticles in polymer matrix [20–22]. Therefore, TEM micrographs of TiO_2, ASA and TiO_2/ASA nanocomposites were acquired and illustrated in Fig. 1. Clearly, the images at the high magnification provide a good evaluation about particle size and morphology, especially the dispersibility of TiO_2. Compared with Fig. 1b, the dark parts in Fig. 1c–e can refer to the TiO_2 nanoparticles as the atomic number of Ti is much higher [23]. When the TiO_2 content is 1 wt%, it presents a uniform dispersion in ASA, and the TiO_2 particles are encapsulated in ASA as shown in Fig. 1c. With the increasing loading content of TiO_2, the dispersibility of TiO_2 declines because some of TiO_2 nanoparticles begin to agglomerate as can be seen from Fig. 1d and e. Especially in Fig. 1e, where relatively larger dark parts can be obviously observed, and these large dark parts are mainly caused by the relatively serious agglomeration of TiO_2 nanoparticles.

3.2. FTIR analysis

To reveal the interactions between TiO_2 and ASA chains, FTIR spectra of TiO_2, ASA and TiO_2/ASA nanocomposites in the range 4000–400 cm^{-1} are shown in Fig. 2. The bands at 2931 and 1452 cm^{-1} are associated with the C-H asymmetric stretching and bending vibration in methylene group, as well as 2874 and 1376 cm^{-1} are C-H symmetric deformation in methyl group [24,25]. The bands at 1735 and 2238 cm^{-1} are respectively attributed to the stretching vibration of carbonyl (C═O) [26–28] and cyano (C≡N) [29,30]. Moreover, the absorption peaks at 703 and 1602 cm^{-1} are indicative of single substituted phenyl ring and vibration of benzene skeletal ring, respectively [31]. Note that the broad peak below 700 cm^{-1} on TiO_2 curve is assigned to Ti–*O*–Ti bond [32], and it should have been appeared on the TiO_2/ASA curves. However, no significant changes has been observed comparing ASA curve with TiO_2/ASA curves. The reasons may be as follows. Since the density of TiO_2 is much higher than ASA, the volume percent of TiO_2 is much smaller, even less than 1 vol% of ASA. Besides, there are also some sharp peaks on ASA curve below 700 cm^{-1} and the peak positions of them are close to that of Ti–*O*–Ti bond. Therefore, the broad peak of Ti–*O*–Ti bond is difficult to be observed on TiO_2/ASA curves.

3.3. WAXD analysis

In order to confirm that the crystal form of rutile TiO_2 remains

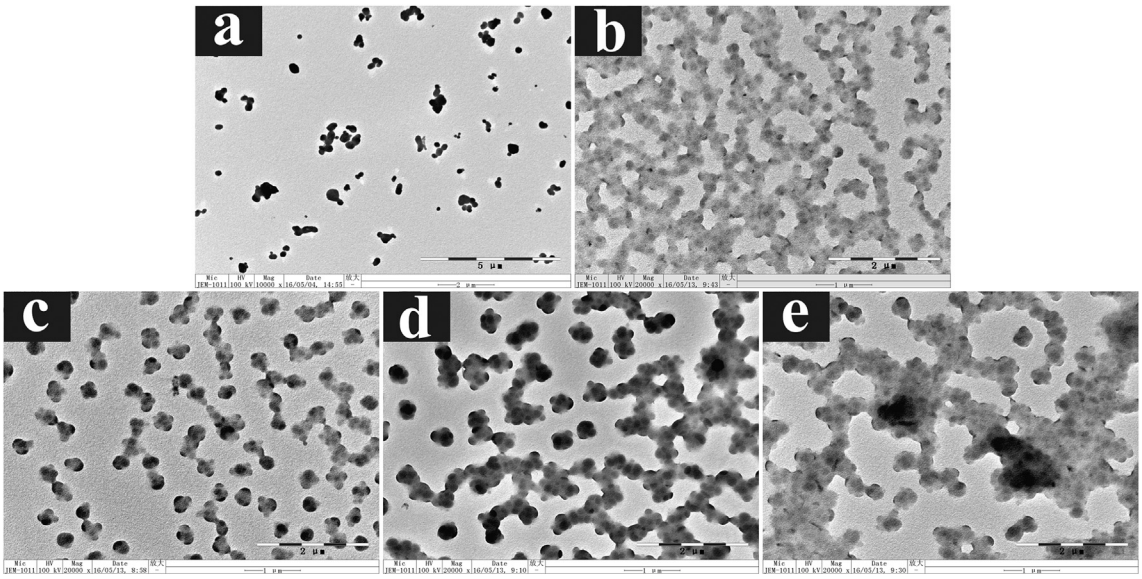

Fig. 1. TEM micrographs of TiO_2, ASA and TiO_2/ASA nanocomposites: (a) TiO_2, (b) ASA, (c) (1 wt%)TiO_2/ASA, (d) (2 wt%)TiO_2/ASA, (e) (3 wt%)TiO_2/ASA. (The magnification of a is 10,000 × and b-e is 20,000 × .)

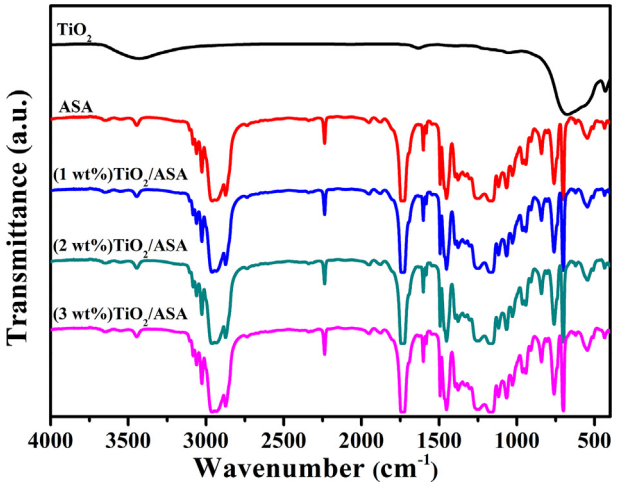

Fig. 2. FTIR spectra of TiO_2, ASA and TiO_2/ASA nanocomposites.

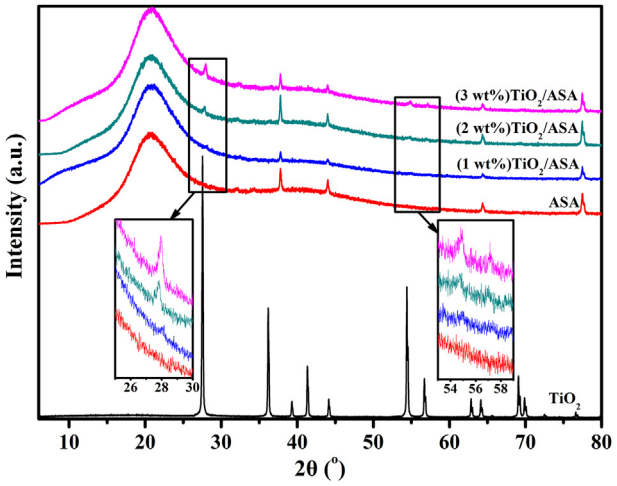

Fig. 3. WAXD patterns for TiO_2, ASA and TiO_2/ASA nanocomposites. Note that the sharp peaks at about 38°, 44°, 64° and 78°are due to the aluminum sample holder.

unchanged before and after the emulsion polymerization, WAXD measurement was performed. WAXD diffraction patterns for TiO_2, ASA and TiO_2/ASA nanocomposites in the range 5-80° are sketched in Fig. 3. The broad peak between 15 and 25° is resulted from the amorphous structure of ASA. Comparing TiO_2/ASA nanocomposites with the neat ASA, some new diffraction peaks appear at about $2\theta = 27.5$, 54.5 and 56.8°, which can be ascribed to the addition of rutile TiO_2 and indicates that the crystal form of TiO_2 is not affected by the emulsion polymerization process.

3.4. Mechanical properties

In order to evaluate the influence of the introduced TiO_2 via in situ polymerization on the mechanical properties of TiO_2/ASA nanocomposite, both impact toughness and tensile properties were measured. Fig. 4 exhibits the impact properties of ASA and TiO_2/ASA nanocomposites. Interestingly, the introduction of TiO_2 induces a significant improvement in the impact toughness of TiO_2/ASA nanocomposites. The impact strength increases dramatically from 22.6 kJ/m^2 to 33.4 kJ/m^2 when the TiO_2 content is 1 wt%. This remarkable improvement can be attributed to the following reasons. The in situ polymerization process leads to a better dispersibility of TiO_2 in ASA matrix according to the result of TEM analysis. As reported, during the fracture of a nanocomposite, the stress will have to be larger to start the microcrack on nanoparticle, and the impact energy will largely be absorbed by the exhibited plastic deformation which occurs more easily around the nanoparticles [33,34]. Therefore, the better dispersibility of TiO_2 in ASA matrix indeed results a better impact strength, which mainly owes to the ultrasonic dispersion before polymerization as described in Scheme 1. Besides, with the increasing content of TiO_2, the impact strength shows a slight decline which is mainly due to the agglomeration of TiO_2 nanoparticles as shown in TEM micrographs.

The tensile properties of ASA and TiO_2/ASA nanocomposites are illustrated in Fig. 5. Traditionally, the introduction of rigid inorganic nanoparticles tends to increase the stiffness of the nanocomposite but decrease its strength and elongation at break [35]. However,

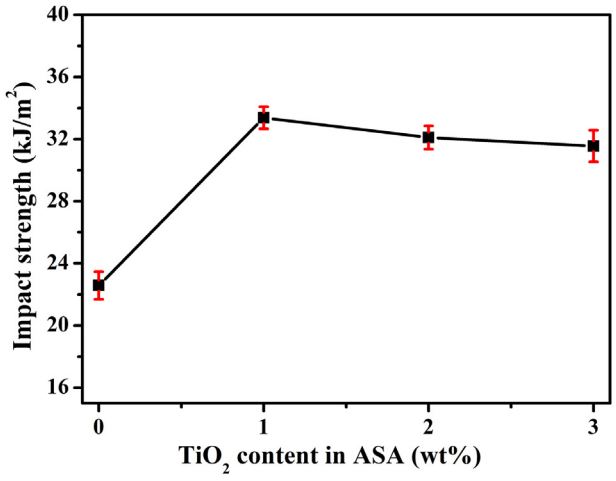

Fig. 4. Impact strength of ASA and TiO_2/ASA nanocomposites.

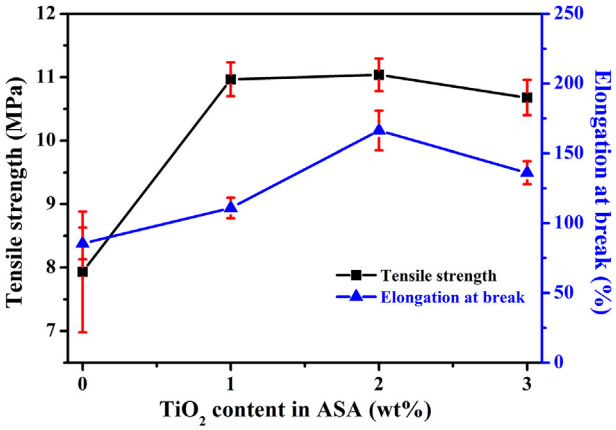

Fig. 5. Tensile properties of ASA and TiO_2/ASA nanocomposites.

both the tensile strength and elongation at break increase with the introduction of TiO_2. The increased tensile strength can be attributed to the better dispersibility of TiO_2 in ASA matrix resulted from the in situ polymerization. Because of the high specific surface area, TiO_2 nanoparticles create a large interfacial area, which provides TiO_2/ASA nanocomposites the increased tensile strength by transferring stresses and elastic deformations from the ASA matrix to TiO_2 nanoparticles [36,37].

3.5. SEM analysis

It is well known that the morphology is usually the key factors to influence the materials' mechanical properties. And SEM analysis is usually performed to investigate the morphology of materials. The SEM micrographs of impact fractured surfaces of ASA and TiO_2/ASA nanocomposites are exhibited in Fig. 6. Firstly, We focus on the micrographs at low magnification (× 3000). Comparing with Fig. 6a, Fig. 6b–d presents different fractured morphology that more root-like whiskers appear on the fractured surface of TiO_2/ASA nanocomposites. This morphology is probably related to the addition of TiO_2 and to some extent, this change of the fractured morphology might be the reason for the dramatical increase of the impact strength. Then, we change our focus to the micrographs at high magnification (×20,000). Strangely, compared with Fig. 6a, no obvious TiO_2 nanoparticles can be observed in Fig. 6b–d. However, we can see some other changes. Compared with Fig. 6a, Fig. 6b–d shows different fracture morphologies with some raised parts. This can be explained as follows. The in situ polymerization process makes TiO_2 nanoparticles be encapsulated in ASA molecular chains, just as the reaction product presented in Scheme 1 and the TEM micrographs can prove this. When TiO_2/ASA nanocomposites break, TiO_2 nanoparticles are still encapsulated in ASA molecular chains instead of being stripped from the ASA molecular chains, which results in the different fracture morphologies with some raised parts.

3.6. Cooling properties

3.6.1. Solar reflectance

The solar reflectance is a very important property for a cooling material which can indirectly reflect the cooling efficiency. Fig. 7 shows the solar reflectance of ASA and TiO_2/ASA nanocomposites. Significant absorptions can be seen above 1000 nm due to mid-IR overtones of carbon hydrogen single bond vibrations and below 300 nm due to the carbonyl group of ASA [38]. Obviously, the solar reflectance of the neat ASA is higher than that of TiO_2/ASA nanocomposites in ultraviolet region due to the strong absorption effect on ultraviolet light of rutile TiO_2, which is of great importance to protect materials from ultraviolet light externally [17,18]. However, in the visible and near infrared region, the neat ASA has shown the lowest reflectance curve compared with other nanocomposites, indicating TiO_2 nanoparticles linearly improve the solar reflectance of ASA.

The irradiance-weighted average reflectance values calculated using Eqs. (1)–(2) are displayed in Table 2. In ultraviolet region, TiO_2/ASA nanocomposites exhibit lower reflectance than that of the neat ASA, which is consistent with the reflectance curves and ascribed to the same reason. And the higher the content of TiO_2, the lower the reflectance of nanocomposite. Since the vibration of the carbon and the hydrogen results in a large inevitable absorption of the light, the reflectance value in near infrared is much lower than that in the visible region. In addition, the reflectance value increases with the increasing content of TiO_2 both in visible and near infrared region. Moreover, the weight of visible and near infrared region covers the most part of the solar spectrum, the total solar reflectance R_{sol} depends on the visible R_v and near infrared R_n parts. Undoubtedly, the nanocomposites have higher total solar reflectance than the neat ASA.

3.6.2. Temperature test

The temperature test can quantitatively reflect the real cooling property of the samples [14]. Fig. 8 illustrates the temperature change of the inner space of the device versus time interval. Overall, the internal temperature rises at a gradually declining rate with the increasing time and levels off eventually. As predicted, the internal temperature of the empty device increases to the highest due to direct solar radiation without any obstruction. By contrast, the internal temperature of the device covered with the neat ASA sample presents a much smaller increase, nearly 10 °C lower than that of the empty device, which indicates that the neat ASA itself has a good cooling property. This is perhaps due to two reasons. One is that ASA is a kind of opaque material which leads less visible light to transmit. But we are inclined to the second explanation: the solar reflectance of ASA is rather high which is 46.75%, nearly half of the total. Even so, the contribution of TiO_2 to improving the cooling property of ASA can be still reflected. As we can see, the temperature curve of TiO_2/ASA nanocomposites is lower than that of the neat ASA, which is consist with the solar reflectance values in Table 1.

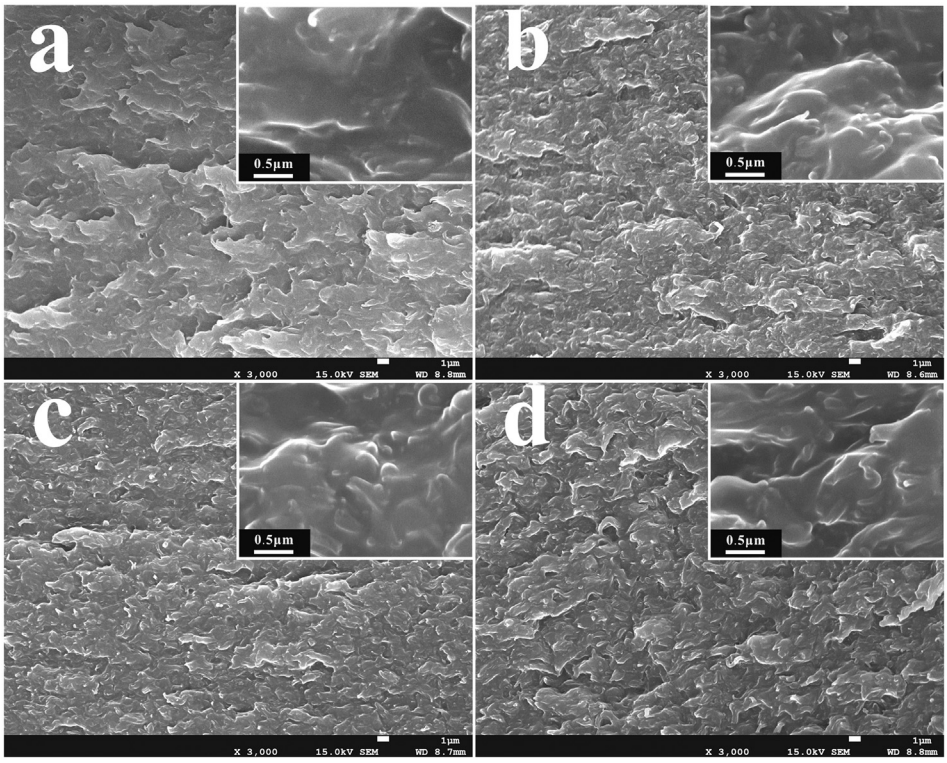

Fig. 6. SEM micrographs of ASA and TiO_2/ASA nanocomposites: (a) neat ASA, (b) (1 wt%)TiO_2/ASA, (c) (2 wt%)TiO_2/ASA, (d) (3 wt%)TiO_2/ASA. (The magnification of the top-right insets is 20,000 × .)

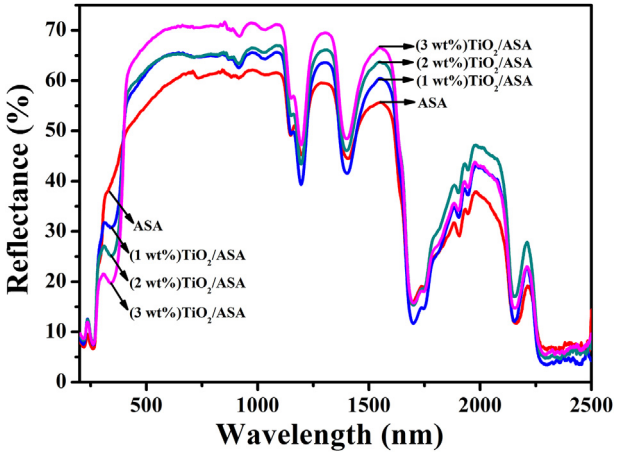

Fig. 7. Solar reflectance of ASA and TiO_2/ASA nanocomposites.

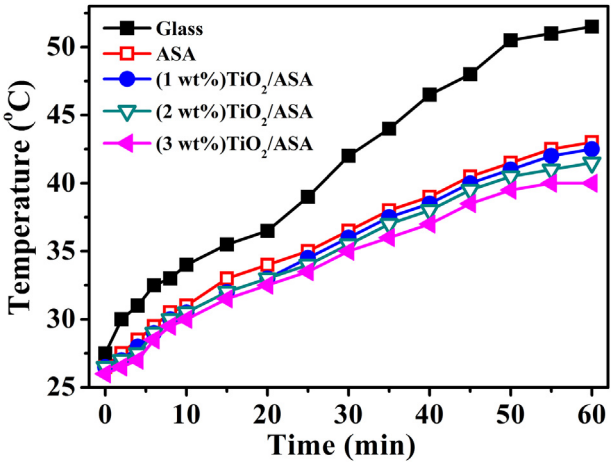

Fig. 8. The temperature change of the inner space of the device versus time interval. This temperature test is measured from 12:00–13:00 on 14th August 2015, the real-time temperature of environment 32 °C, 32°4′37″N, 118°46′19″E, in city Nanjing, China.

Table 2
Detailed irradiance-weighted average values of ASA and TiO_2/ASA nanocomposites.

Samples	R_u (%)	R_v (%)	R_n (%)	R_{sol} (%)
ASA	38.03	56.80	39.27	46.75
(1 wt%)TiO_2/ASA	32.97	62.42	40.85	49.73
(2 wt%)TiO_2/ASA	28.71	62.79	43.73	51.17
(3 wt%)TiO_2/ASA	23.86	67.76	44.89	53.67

All reflectance values of different bands (R_u, R_v, R_n) were calculated by Eq. (1), the total solar reflectance values R_{sol} was calculated by Eq. (2).

4. Conclusions

TiO_2/ASA nanocomposites with different loading content of TiO_2 were prepared by in situ emulsion polymerization. The result of WAXD analysis indicated that the crystal form of TiO_2 was not affected by the emulsion polymerization process. Interestingly, the introduction of TiO_2 induced a significant improvement in the impact toughness of TiO_2/ASA nanocomposites, which increased dramatically by about 10 kJ/m^2. And we attributed this improvement to the better dispersibility of TiO_2 in ASA matrix which is

proved by TEM analysis. Besides, the solar reflectance of the nanocomposites was related to the addition of TiO_2 nanoparticles. And the more the TiO_2 nanoparticle was added, the higher the solar reflectance of the composite was. Moreover, the outdoor temperature test just proved the result of the solar reflectance.

Acknowledgements

This work was supported by the Innovation Foundation for Graduate Students of Jiangsu Province (KYZZ15_0222) and the Priority Academic Program Development of Jiangsu Higher Education Institutions (PAPD).

References

[1] Silani M, Ziaei-Rad S, Esfahanian M, Tan VBC. On the experimental and numerical investigation of clay/epoxy nanocomposites. Compos Struct 2012;94(11):3142–8.
[2] Pavlidou S, Papaspyrides CD. A review on polymer-layered silicate nanocomposites. Prog Polym Sci 2008;33(12):1119–98.
[3] Wang Y, Shen Y, Pei X, Zhang S, Liu H, Ren J. In situ synthesis of poly(styrene-co-maleic anhydride)/SiO_2 hybrid composites via "grafting onto" strategy based on nitroxide-mediated radical polymerization. React Funct Polym 2008;68(8):1225–30.
[4] Vodnik VV, Božanić DK, Džunuzović E, Vuković J, Nedeljković JM. Thermal and optical properties of silver-poly(methylmethacrylate) nanocomposites prepared by in situ radical polymerization. Eur Polym J 2010;46(2):137–44.
[5] Zakaria MR, Akil HM, Kudus MHA, Kadarman AH. Improving flexural and dielectric properties of MWCNT/epoxy nanocomposites by introducing advanced hybrid filler system. Compos Struct 2015;132:50–64.
[6] Choi J, Shin H, Yang S, Cho M. The influence of nanoparticle size on the mechanical properties of polymer nanocomposites and the associated interphase region: a multiscale approach. Compos Struct 2015;119(119):365–76.
[7] Zhao J, Milanova M, Warmoeskerken MMCG, Dutschk V. Surface modification of TiO_2 nanoparticles with silane coupling agents. Colloids Surf A 2012;413(21):273–9.
[8] Li XW, Song RG, Jiang Y, Wang C, Jiang D. Surface modification of TiO_2 nanoparticles and its effect on the properties of fluoropolymer/TiO_2 nanocomposite coatings. Appl Surf Sci 2013;276(3):761–8.
[9] Zhang W, Zhang J. Toughening effect of PNBR on ASA/SAN binary blends. J Vinyl Addit Technol 2014;20(4):268–74.
[10] Han Y, Tai ZX, Zhou C, Zhang MY, Zhang HX, Liu FQ. Influence of blend composition on the mechanical properties and morphology of PC/ASA/SAN ternary blends. Polym Bull 2009;62(6):855–66.
[11] Sokhandani P, Babaluo AA, Rezaei M, Shahrezaei M, Hasanzadeh A, Mehmandoust SG, et al. Nanocomposites of PVC/TiO_2 nanorods: surface tension and mechanical properties before and after UV exposure. Addict Biol 2013;129(6):3265–72.
[12] Wang S, Zhang J. Non-isothermal crystallization kinetics of high density polyethylene/titanium dioxide composites via melt blending. J Therm Analysis Calorim 2014;115(1):63–71.
[13] Ling Z, Wenjun F, Songlin W. Novel photodegradable low-density polyethylene-TiO_2 nanocomposite film. Environ Sci Technol 2006;40(5):1681–5.
[14] Wang S, Zhang J. Influence of titanium dioxide content on the crystallization behavior and solar reflectance of polyethylene/titanium dioxide composites. Int J Polym Anal Ch 2014;19(4):287–95.
[15] Zhu Y, Allen GC, Adams JM, Gittins D, Heard PJ, Skuse DR. Statistical analysis of particle dispersion in a PE/TiO_2 nanocomposite film. Compos Struct 2010;92(9):2203–7.
[16] Xu H, Shi T, Sun J, Yang Z. Preparation,characterization and properties of butyl acrylate-styrene-acrylonitrile copolymer/titanium dioxide composite film. China Synth Rubber Ind 2011;34(4):282–6.
[17] Levinson R, Berdahl P, Akbari H, Miller W, Joedicke I, Reilly J, et al. Methods of creating solar-reflective nonwhite surfaces and their application to residential roofing materials. Sol Energ Mater Sol C 2007;91(4):304–14.
[18] Wang S, Zhang J. Effect of nucleating agent on the crystallization behavior, crystal form and solar reflectance of polypropylene. Sol Energ Mater Sol C 2013;117(4):577–84.
[19] Xiang B, Qi Y, Wang S, Zhang J. Using a novel and easy-to-use sandwich structure device to evaluate the cooling properties of cool materials. Int J Polym Anal Ch 2015;20(6):529–40.
[20] Ramesh S, Sivasamy A, Rhee KY, Park SJ, Hui D. Preparation and characterization of maleimide-polystyrene/SiO_2-Al_2O_3 hybrid nanocomposites by an in situ sol-gel process and its antimicrobial activity. Compos Part B Eng 2015;75(2):167–75.
[21] Gong X, Pan L, Tang CY, Chen L, Hao Z, Law WC, et al. Preparation, optical and thermal properties of CdSe–ZnS/poly(lactic acid) (PLA) nanocomposites. Compos Part B Eng 2014;66(4):494–9.
[22] Gong X, Tang CY, Pan L, Hao Z, Chi PT. Characterization of poly(vinyl alcohol) (PVA)/ZnO nanocomposites prepared by a one-pot method. Compos Part B Eng 2014;60(2):144–9.
[23] Bals S, Kabius B, Haider M, Radmilovic V, Kisielowski C. Annular dark field imaging in a TEM. Solid State Commun 2004;130(10):675–80.
[24] Rong Q, Zhu A, Zhong T. Poly (styrene-n-butyl acrylate-methyl methacrylate)/silica nanocomposites prepared by emulsion polymerization. J Appl Polym Sci 2011;120(6):3654–61.
[25] Malas A, Pal P, Giri S, Mandal A, Das CK. Synthesis and characterizations of modified expanded graphite/emulsion styrene butadiene rubber nanocomposites: mechanical, dynamic mechanical and morphological properties. Compos Part B Eng 2014;58(3):267–74.
[26] Qin L, Qiu J, Liu M, Ding S, Shao L, Lü S, et al. Mechanical and thermal properties of poly (lactic acid) composites with rice straw fiber modified by poly (butyl acrylate). Chem Eng J 2011;166(2):772–8.
[27] Guo Y, Li S, Wang G, Ma W, Huang Z. Waterborne polyurethane/poly (n-butyl acrylate-styrene) hybrid emulsions: Particle formation, film properties, and application. Prog Org Coat 2012;74(1):248–56.
[28] Tan QC, Shanks RA, Hui D. Functionalised graphene-multiwalled carbon nanotube hybrid poly(styrene-b-butadiene-b-styrene) nanocomposites. Compos Part B Eng 2016;90(1):315–25.
[29] Bittmann B, Haupert F, Schlarb AK. Preparation of TiO_2 epoxy nanocomposites by ultrasonic dispersion and resulting properties. J Appl Polym Sci 2012;124(3):1906–11.
[30] Samaržija-Jovanović S, Jovanović V, Marković G, Konstantinović S. Nanocomposites based on silica-reinforced ethylene–propylene–diene–monomer/acrylonitrile–butadiene rubber blends. Compos Part B Eng 2011;42(42):1244–50.
[31] Parashar P, Ramakrishna K, Ramaprasad AT. A study on compatibility of polymer blends of polystyrene/poly(4-vinylpyridine). J Appl Polym Sci 2011;120(3):1729–35.
[32] Nguyen VG, Thai H, Mai DH, Tran HT, Dai LT, Vu MT. Effect of titanium dioxide on the properties of polyethylene/TiO 2 nanocomposites. Compos Part B Eng 2013;45(1):1192–8.
[33] Zhang J, Xin W, Lu L, Dan L, Yang X. Preparation and performance of high-impact polystyrene (HIPS)/nano-TiO_2 nanocomposites. J Appl Polym Sci 2003;87(3):381–5.
[34] Rösch J, Mülhaupt R. The role of core/shell-microparticle dispersions in polypropylene/polyamide-6 blends. Polym Bull 1994;32(5–6):697–704.
[35] Nicolais L, Narkis M. Stress-strain behavior of styrene-acrylonitrile/glass bead composites in the glassy region. Polym Eng Sci 1971;11(11):194–9.
[36] Chuayjuljit S, Neeranatmanit K, Boonmahitthisud A. Property improvement of plasticized poly(vinyl chloride) by nano-TiO_2 and poly(methyl methacrylate)-encapsulated nano-TiO_2. J Vinyl Addit Technol 2015 . http://dx.doi.org/10.1002/vnl.21462.
[37] Carballeira P, Haupert F. Toughening effects of titanium dioxide nanoparticles on TiO_2/epoxy resin nanocomposites. Polym Compos 2010;31(31):1241–6.
[38] Oreski G, Tscharnuter D, Wallner GM. Determination of solar optical properties of transparent polymer films using UV/vis spectroscopy. Sol Energ Mater Sol C 2010;94(5):884–91.